Soot on snow experiment: bidirectional reflectance factor measurements of contaminated snow

J. I. Peltoniemi[1,2], M. Gritsevich[1,2,7], T. Hakala[1], P. Dagsson-Waldhauserová[5,6],
Ó. Arnalds[6], K. Anttila[1,3], H.-R. Hannula[4], N. Kivekäs[3], H. Lihavainen[3],
O. Meinander[3], J. Svensson[3,8], A. Virkkula[3], and G. de Leeuw[2,3]

[1]Finnish Geospatial Research Institute (FGI) (former Finnish Geodetic Institute), Geodeetinrinne 2, Masala, Finland
[2]Department of Physics, University of Helsinki, P.O. Box 64, Helsinki, Finland
[3]Finnish Meteorological Institute, P.O. Box 503, Helsinki, Finland
[4]Finnish Meteorological Institute Arctic Research Centre, Tähteläntie 62, Sodankylä, Finland
[5]University of Iceland, Department of Physics, Reykjavik, Iceland
[6]Agricultural University of Iceland, Faculty of Environment, Hvanneyri, Iceland
[7]Ural Federal University, Institute of Physics and Technology, Ekaterinburg, Russia
[8]Department of Environmental Science, University of Helsinki, Helsinki, Finland

Correspondence to: J. I. Peltoniemi (jouni.peltoniemi@helsinki.fi)

Abstract. In order to quantify the effects of absorbing contaminants on snow, a series of spectral reflectance measurements were conducted. Chimney soot, volcanic sand, and glaciogenic silt were deposited on a natural snow surface in a controlled way as a part of the Soot on Snow (SoS) campaign. The bidirectional reflectance factors of these soiled surfaces and untouched snow were

5   measured using the Finnish Geodetic Institute's Field Goniospectropolariradiometer, FIGIFIGO.

A remarkable feature is the fact that the absorbing contaminants on snow enhanced in our experiments the metamorphism of snow under strong sunlight. Immediately after deposition, the contaminated snow surface appeared darker than the natural snow in all viewing directions, but the absorbing particles sank deep into the snow in minutes. The nadir measurement remained the darkest, but at

10   larger zenith angles the surface of the contaminated snow changed back to almost as white as clean snow. Thus, for a ground observer the darkening caused by impurities can be completely invisible, overestimating the albedo, but a nadir observing satellite sees the darkest points, now underestimating the albedo. By a reciprocity argument, we predict, that at noon the albedo perturbation should be lower than in the morning or afternoon. When sunlight stimulates sinking more than melting,

15   the albedo should be higher in the afternoon than in the morning, and vice versa when melting dominates. However, differences in the hydrophobic properties, porosity, clumping, or size of the impurities may cause different results than observed in these measurements.

1 Introduction

Snowpacks and ice sheets around the globe play a crucial role in the Earth's radiation budget. The albedo of snow depends, among other factors, on its physical properties, such as, for example, snow grain size, shape, packing, topography and snow thickness. It is usually significantly higher compared to that of other natural surfaces (Peltoniemi et al., 2015).

With the rapidly growing techniques for Earth observation, the accelerating shrinkage of snowpacks and glaciers over the past decades has been confirmed based on dedicated satellite and in situ measurements. In order to reliably interpret these observations and forecast further changes in snow cover, there is a need to increase existing knowledge on the processes affecting the state of snow. Deposition of light-absorbing impurities on the surface of snow decrease its reflectance (Warren and Wiscombe, 1980; Clarke and Noone, 1985; Dumont et al., 2014) and accelerate snow melt (Bond et al., 2013).

The presence of light-absorbing impurities in the snow may cause dramatic effects even on fresh snow surfaces lowering their reflectivity below the typical range of 0.7–0.9. Aerosol particles originating from both anthropogenic and natural sources can be transported over very long distances.

Measurements of actual impurity concentrations in snowpacks and glaciers have been conducted on different spatial and temporal scales in natural conditions by for example Clarke and Noone (1985); McConnell et al. (2007); Ming et al. (2008); Xu et al. (2009); Forsström et al. (2009); Doherty et al. (2010); Kaspari et al. (2011); Bisiaux et al. (2012); Meinander et al. (2013); Svensson et al. (2013); Dagsson-Waldhauserova et al. (2015). Furthermore, to observe the effects of impurities on the snow, several experimental studies have been conducted (Conway et al., 1996; Brandt et al., 2011; Hadley and Kirchstetter, 2012). Their set-ups have been carefully reviewed by Svensson et al. (2015). The reflectance of natural snow has already been measured in several ways, for instance in Piironen et al. (2000); Aoki et al. (2000); Painter et al. (2003); Kaasalainen et al. (2006); Bourgeois et al. (2006); Peltoniemi et al. (2009); Tanikawa et al. (2014), and that of carbon particles alone by Sasse and Peltoniemi (1995).

The reflectance of natural snow has been modelled by many, using various combinations of radiative transfer, ray-tracing, and electromagnetic techniques (Wiscombe and Warren, 1980; Aoki et al., 2000; Tanikawa et al., 2006; Peltoniemi, 2007; ; Räisänen et al., 2015). Snow contaminated with impurities has been modelled for example by Warren and Wiscombe (1980); Flanner et al. (2007); Kokhanovsky (2013). These models can usually provide a first order approximation for the distribution of the reflected radiation and effects of impurities. However, all the models contain uncertainties in modelling the shape of the snow grains, their size distributions, and 3 dimensional structure of the snow pack and the distribution of impurities. These factors can change the albedo several per cents, and at certain directions the reflectance much over 10 % (Peltoniemi, 2007). None of the models have yet been able to explain the observed polarization features (Peltoniemi et al., 2010b).

The Finnish Meteorological Institute (FMI) organized a series of experiments, using a different approach than the referred studies (Meinander et al., 2014; Svensson et al., 2015). Experiments were conducted in different regions in Finland, in 2011 and 2013, with the general aim to monitor and quantify the effects of soot on the albedo and physical properties of the snowpack. To this end, absorbing aerosols of different origin were deposited on a natural snowpack in a controlled way and the changes in the snow pack properties were measured (Meinander et al., 2014; Svensson et al., 2015). In this paper we describe the measurements of the bidirectional reflectance factor (BRF) used to quantify the effects of different absorbing materials on snow using the Finnish Geodetic Institute's Field Goniospectropolariradiometer, FIGIFIGO.

2 Methods and instruments

The bidirectional reflectance factor (BRF for short, or R in equations) is defined as the ratio of the reflected light intensity of a given target to an ideal Lambertian reflector with a spherical albedo of 1.0 under same incident irradiation (Nicodemus et al., 1977; Hapke, 1993). The BRF can be presented as

$$R(\mu, \mu_0, \phi, \phi_0) = \frac{\pi I(\mu, \phi)}{\mu_0 F_0(\mu_0, \phi_0)}, \tag{1}$$

where F_0 is the incident collimated flux and I the reflected radiance; ι and ϕ_0 are the zenith and azimuth angles of incidence, ϵ and ϕ are the zenith and azimuth angles of emergence, α is the phase angle that is defined as the angle between the source and observer equalling the complement of the scattering angle ($\cos\alpha = \cos\iota\cos\epsilon + \sin\iota\sin\epsilon\cos(\phi - \phi_0)$), and $\mu = \cos\epsilon, \mu_0 = \cos\iota$ (Fig. 1). A related quantity is the bidirectional reflectance distribution function (BRDF), here denoted as $\mathcal{R} = R/\pi$. Experimentalists and practical users prefer using BRF for its more intuitive magnitude which is normalized to a perfect Lambertian reflector $R = 1$. Modellers prefer BRDF for its more natural mathematical interpretation and simpler equations. For example reflected radiation can be written with $\mathcal{R}$ as

$$\begin{aligned} I(\mu, \phi) &= \int d\mu'\phi' \mathcal{R}(\mu, \phi, \mu', \phi')\mu' I(\mu', \phi') \\ &= \int d\mu'\phi' \mathcal{R}(\mu, \phi, \mu', \phi')\mu' I_{\text{Diff}}(\mu', \phi') \\ &\quad + \mathcal{R}(\mu, \phi, \mu_0, \phi_0)\mu_0 F_0(\mu_0, \phi_0), \end{aligned} \tag{2}$$

where I_{Diff} represents diffuse skylight.

For the detailed multi-angular reflectance measurements conducted within the experiment we have used the FIGIFIGO, Finnish Geodetic Institute's Field Goniospectropolariradiometer (Peltoniemi et al., 2009, 2010b, a, 2014; Suomalainen et al., 2009; Hakala et al., 2010, 2014), shown in Fig. 2. The primary sensor of the FIGIFIGO is an ASD FieldSpec Pro FR spectroradiometer (Analytical Spectral Devices Inc.) with a spectral range of 350–2500 nm, full width at half maximum of 3 nm

from 350–1000 nm and 10 nm from 1000–2500 nm. The spectrometer is connected to the front optics with a light cable of a length of 3 m. The optics is interchangeable, including normal optics with a 3° field of view, and optics with a rotatable Glan-Thompson linear polariser.

90   The optics are placed on top of a 1.5–2.5 m long telescope arm. At an arm length of 2.5 m the optics footprint diameter is 20 cm. The arm is equipped with an inclinometer and a motor, which allows changing of the view zenith direction by tilting the arm. The view azimuth angle is selected by turning the whole device manually. In the field conditions the orientation relative to the Sun is measured with a fish-eye camera fixed to the FIGIFIGO frame, and the direction of the Sun is

95   calculated based on GPS positioning and time. The fish-eye camera also saves images of the sky periodically for post-processing sky monitoring purposes. Solar irradiance is additionally monitored by a silicon pyranometer (SP Lite, Kipp and Zonen) during the measurement.

    The FIGIFIGO field measurement process went as follows

1. The target was selected and prepared (see next section for details).

100 2. The system was mounted and started. At least 20 min was allowed for the spectrometer to warm up, in most cases more.

3. The sensor was optimized and a reference measurement taken using a white 25 cm Spectralon panel by Labsphere with a nominal reflectance of 99%. The panel was carefully levelled, and its cleanness checked. Any loose dust or water drops were removed by compressed air.

105 4. The contribution of diffuse light from the sky, clouds, and the environment (M_D in the Eq. (3) below) was measured by shadowing the target from direct sunlight using a small screen.

5. Then, the target reflectance was measured, with automatically turning the zenith arm, and manual azimuthal rotations.

6. The Spectralon white reference was remeasured several times during the measurements and at

110   the end of the sequence, depending on illumination stability.

7. The documentation was completed, the data file was closed, and the system moved to the next target or dismounted.

In laboratory the diffuse part was not needed, but one more step to set-up the illumination with 1000 W QTH lamp by Oriel was required. The data were checked and erratic data removed. Unstable

115 data were marked as unstable. The spectral measurement was normalised with white reference data and the diffuse part subtracted. For unpolarised measurements, the data renormalisation goes as follows

$$R(\mu,\phi,\mu_0,\phi_0) = \frac{M(\mu,\phi,\mu_0,\phi_0) - M_{\mathrm{D}}(1,\mu_0,\phi_0)}{S(\mu,\phi,\mu_0,\phi_0) - S_{\mathrm{D}}(1,\mu_0,\phi_0)} R_{\mathrm{ref}}(\mu,\phi,\mu_0,\phi_0), \tag{3}$$

4

where M is the measurement of the target, M_D the estimate for the diffuse part, S the measurement of the Spectralon standard, S_D the diffuse part of that, and R_{ref} the laboratory–measured value of the reflectance of the Spectralon(Peltoniemi et al., 2014). Because the reference values are not measured simultaneously for each measurement, but only at the start and end (if possible), the reference values were interpolated from the nearest points based on time. The diffuse light estimate is based on nadir measurement only, yielding a 1–5 % uncertainty concentrating in the blue end. With polarisation the procedure involved more phases, but here polarisation data are not shown.

3   Samples

The major contributions to the absorption of light in nature originate from volcanic sand, glacionegic silt and natural and anthropogenic sources of black and brown carbon. For the purposes of our experiment, the components described below were primarily selected. See also Table 1 and Fig. 3.

3.1   Volcanic sand

Volcanic sand was collected from the Myrdalssandur dust source in the Southern Iceland in November 2012. This material has been mixed by aeolian processes, resulting in an enriched sand proportion as the silt sized material is lost as dust along the way. The sample is a near black mixture of volcanic ash of glaciofluvial nature, originating from under the Myrdalsjokull glacier, which may be mixed with the ash of the Eyjafjallajokull eruption in 2010 and the Grimsvotn eruption in 2011. It represents well the material re-suspended in the most active dust source in Southern Iceland and deposited on glaciers or snow in South and South–East Iceland. Atmospheric dust in Iceland comes from two different dust sources. The first are the extensive sandy deserts. Many of these produce little dust per unit area (very variable because of many types of sandy surfaces), but due to their extent, they are an important dust source. The second main source of dust from Iceland are dust plume areas with high dust productivity per unit area, located mostly near glaciers and along glacial river beds. The volcanic dust is mostly made of basaltic to andesitic poorly crystallized glass particles, dark to black in colour. The density is about $0.9 \, \mathrm{kg} m^3$.

3.2   Glaciogenic silt

The sample was collected from the glacial river Mulakvisl, about $10 \, \mathrm{km}$ from the Myrdalsjokull glacier in Southern Iceland, one of the main rivers draining the glacier, and the materials originates from the Katla volcanic system under the glacier. The glaciogenic silt is brighter in colour than the sand. It is light-brown to slightly yellowish in colour and it consists mainly of silt and some coarse clay sized particles, which are easily re-suspended on daily basis on dry days. This material can be transported and deposited on the local glaciers as well as being transported by wind several hundreds of kilometres towards Europe. The density is about $1.2 \, \mathrm{kg} m^3$.

5

3.3 Chimney soot

Soot was acquired from a chimney-sweeping company in Helsinki, which collected the soot from residential buildings using small-scale wood and oil burning as heating. The soot was blown onto the snow surface as explained by Svensson et al. (2015). Here the soot was used as a proxy of black carbon and also containing some brown carbon.

3.4 Contaminated snow in Sodankylä

The main experiment series of the SoS 2013 campaign took place in Sodankylä airport, Northern Finland, where specific set-ups had been build already before snow fall. In order to control the absorption in snow, the above described contaminants were deposited on snow in various ways. The main experiment and the soot depositing system are described in Svensson et al. (2015). In short, the soot was fed to a cyclone separating smaller particles to be blown into a closed chamber around the target snow where the soot slowly deposited onto the snow surface. Only one preliminary test spot made this way could be measured by FIGIFIGO. However, because the sampling area of FIGIFIGO is much smaller than that of the albedometers, it was possible to use different techniques. For most FIGIFIGO measurements, the particles were distributed manually over an area of $0.5\,\mathrm{m}^2$ using a salt shaker filled with a measured amount of soot.

On the first measurement day of the campaign, 3 April 2013, a clean and smooth snow spot was selected, and its BRF was measured. After that, $8\,\mathrm{g}$ of black volcanic sand was spread manually on the snow over about $0.5\,\mathrm{m}^2$, and the BRF was measured as quickly as possible. The measurement was repeated in the next spot similarly with $8\,\mathrm{g}$ of ash spread over $0.5\,\mathrm{m}^2$. The properties of the clean snow nearby are shown in Tables 2 and 3, with some photographs in Fig. 4.

During the same day (3 April), the primary experiment made its first large test spot using chimney soot. At night, a thin layer of new snow fell over the site, and also all the target spots were covered. In the morning the sky cleared, and a modest wind partially cleaned the fallen snow. The BRF of this sooted sample was measured four times on the 4 April, at different solar zenith angles, also with polarisation, examining the metamorphism process. After the sooted spot, clean untouched snow was measured nearby as a reference. Some profile pictures are shown in Fig. 5.

The measurement continued by depositing $10\,\mathrm{g}$ of glaciogenic silt over an area of $0.5\,\mathrm{m}^2$ of clean snow. Again some sinking happened, but the measurement was fast and the results are considered useful. After some time, another $10\,\mathrm{g}$ was spread over the same spot to make it darker, and the target was measured again.

The sample remained untouched during the night, and the next morning it was measured again. This day (5 April) was already more cloudy than the preceding ones, adding too much uncertainty to perform low concentration measurements. Thus we deposited another $20\,\mathrm{g}$ of silt over the same sample, and measured the reflectance, followed by a clean snow taken for a reference, and again

6

a new sample of snow with $40\,\text{g}$ of silt deposited over an area of $0.5\,\text{m}^2$. The properties of the clean snow nearby are shown in Tables 4 and 5, with some photographs in Fig. 6.

The air temperature varied between $-20\,^{\circ}\text{C}$ at nights and $+5\,^{\circ}\text{C}$ at warmest sunshine. The clean snow temperature was several degrees below zero, from -8 to $-3\,^{\circ}\text{C}$ near the surface and around $-2\,^{\circ}\text{C}$ near bottom. Figure 7 shows the snow and air temperatures measured at a nearby swamp by an FMI weather station. The actual temperatures at the airport site may differ a small amount.

4 Results

The key results are shown in Figs. 9 to 12. Most of the features are shown in three different plots of selected measurements: Left: the BRF as a function of observer zenith and azimuth angles, integrated over the full measurement range weighed with a fixed solar spectrum, gives a good overview of the reflected energy distribution. Middle: the principal plane BRF curve as a function of the observer zenith angle gives more details of the directional effects, here shown in six different wavelength bands: violet $443\,\text{nm}$, green $565\,\text{nm}$, red $670\,\text{nm}$, NIR $865\,\text{nm}$, SWIR $1250\,\text{nm}$, and SWIR $1555\,\text{nm}$, each with a bandwidth of $20\,\text{nm}$ in visual and $50\,\text{nm}$ in IR. Right: the spectral albedo integrated over all directions using semi-polynomial inter/extrapolation is compared with the nadir spectrum. Full data with many different plots can be downloaded at our web site[1]. The first set (Fig. 9) shows the 3 April 11:33 EET measurement of clean snow, the 12:25 measurement of the snow contaminated by $8\,\text{g}$ of volcanic sand per $0.5\,\text{m}^2$, then the 13:22 measurement with $8\,\text{g}$ of volcanic sand per $0.5\,\text{m}^2$, and last the pure volcanic sand sample measured at the laboratory. The second set (Fig. 10) shows the measurements from a sooted snow sample on 4 April at 9:56, and at 11:38, natural snow at 13:31, and the laboratory measurement of pure soot. The 12:39 results are similar to the 11:18 measurements, and are not shown. During the 10:31 measurement, changes were too large to get a full data set. The third set (Fig. 11) shows the effects of fine silt on snow, first $10\,\text{g}$ of silt per $0.5\,\text{m}^2$ on the 4 April at 15:05, then $40\,\text{g}$ of silt per $0.5\,\text{m}^2$ at 16:29, the third same sample on the 5th of of April at 11:16, and last the pure silt measured in the laboratory. In the laboratory, about 1 cm thick layer of the material was spread evenly on a black surface.

To demonstrate the fast metamorphism and sinking effects, Fig. 12 shows data from three measurements, first the principal plane BRF taken at the beginning of the measurement, second the principal plane BRF at the end of the measurement, and finally a time plot of all nadir BRF during one measurement's sequence. The measurements of clean snow on the 5 April started at 15:08, snow with $40\,\text{g}$ of silt on the 5 April at 14:06, and the same $40\,\text{g}$ of silt at a larger zenith angle started at 16:55.

---

[1]https://webdisk.kotisivut.com/fgi/Reflectance_Library

5 Discussion

220 The BRF of snow has been well characterized by many authors, see e.g. review of Peltoniemi et al. (2010b). The spectral shape is strongly influenced by the grain size, and weakly by the presence of liquid water, impurities and the surface below. Directionally, snow is a forward scatterer, with a weak bowl shape in the visible band, and a much deeper bowl in the NIR bands. The directional dependence is most related to the grain shape and topography. Rough snow surfaces scatter more 225 backwards and less sideways than smooth surfaces. Also the irregularity of grains increases the backscattering slightly. The present results don't contradict this. Below, the new effects of impurities are analysed in more detail.

Typically, contaminated snow darkens the most in the nadir, and the least in the forward direction. Especially, when the black contaminants sink deeper into the snow, the bowl shape of the BRF is 230 enhanced, and from larger zenith angles the snow looks brighter. Thus, from the normal human feet-on-ground-perspective, the differences between dirty and clean snow almost disappear, while from the nadir the dirty snow can still be almost black. The directional effects of contaminants are clearly distinguishable from grain size, shape and topography effects only when the concentration of impurities is high and the surface is visibly darker. At more natural $<$ ppm concentrations the 235 directional effect is probably in the limit of significance. The strong forward spike in the 4 April 9:56 measurement (Fig. 10, top) is typical for lower solar angles (here 68°), but may have been enhanced by a tiny amount of fresh snow. Another angular effect may be seen between in the 4 April 16:30 measurement with a starting SZA of 72° and the 5 April 11:56 measurement starting at 61°. At the SZA of 72° the albedo appears clearly brighter than at 61°. Although this may well be only 240 a result of metamorphism during the night, it also fits the pattern that high sun encounters more dark impurities than low sun, if the heating sinks dark material down.

Spectrally, the contaminants darken the snow mostly in the visual bands. The soot, silt and volcanic sand used here have a smooth (grey) spectrum without significant features. The volcanic sand is darker than snow in all wavelengths (Fig. 9), while the silt may be even brighter in the deep- 245 est absorption bands of snow around 1500 and 2000 nm. As expected, at these dark bands the silt contaminated snow is brighter than the cleaner snow (Fig. 11). Thus, a spectral signal for impurity inversion exists, but care is needed to separate it from the grain size effect.

From the data, especially Fig. 12, one can see that also the clean snow varies. The reflectance can change by $\pm 10\%$ in a short time, due to metamorphism. It is not possible to say how clean the clean 250 snow really is. In any case too clean to observe the impurities, but quite likely some of the deposited dust may have landed on the clean snow samples, and all possible aerosol and human and animal traces cause unknown perturbations. An important observation is, however, that adding absorbing impurities enhance melting and metamorphism remarkably. Heated by the sun, the small particles can melt the snow around them, letting them fall down or float up at least several cm, depending on

255 their physical properties. This process happens in minutes, and it is thus impossible to say exactly, what was the state of a sample when measured.

6 Conclusions

A field experiment was made to study the effects of different kinds of impurities on the reflectance of snow. Soot collected from chimneys, volcanic sand, and glaciogenic silt were deposited on natural
260 snow surfaces. This simulates both anthropogenic and natural sources, both being of importance (Dagsson-Waldhauserova et al., 2015). The bidirectional reflectance factor (BRF) was measured using the Finnish Geodetic Institute field goniospectropolariradiometer FIGIFIGO.

Impurities make snow darker. However, the concentrations must be rather significant or the spectral signal strong to separate the effects of the contaminants from other snow variations, such as grain
265 size, surface roughness, or snow pack structures, from reflectance data. Typical natural concentrations of black carbon are less than ppm, which cannot be detected from optical satellite data without additional information, as already pointed out by Warren (2013).

Dark snow is unstable. When the Sun heats the abosrbing particles, they melt or soften the ice around, allowing the particles to move inside the snow. In this experiment, the particles sank down,
270 leaving the topmost (mm to cm scale) surface whiter. Also, snow grain size, shape, density, and surface roughness changed visually. These metamorphism and sinking processes are so fast that it is difficult to link successive measurements to each others, and know what was really measured.

After the sinking, the difference between contaminated and clean snow is largest from nadir, where one can still see the dark contaminants through the sink holes, and smallest at large zenith angles,
275 where one sees mostly pure snow. Also the solar zenith angle has a significant effect on what is seen. At small solar zenith angles light goes deeper inside and may interact more with sunk in impurities than at large zenith angles.

However, different melting conditions, or different hydrophobic properties of the contaminants, may reverse the process, accumulating the dirt on the surface (Conway et al., 1996; Meinander et al.,
280 2014). Such snow was not measured here, and must be studied more before wide conclusions are drawn. But in both cases, models assuming homogeneous distribution of absorbers may over- or underestimate the effect of impurities on the albedo and climate quite significantly.

This experiment aims to fill the gap between laboratory experiments (where one can control the target and measurements optimally) and natural observations (where one measures the targets as they
285 are). In all, we conclude that for modelling snow melt and spectral albedo affected by light-absorbing impurities, more experimental results are needed.

7 Supporting information

All the measurement data are stored in FGI's Reflectance Library and are available at https://webdisk.kotisivut.com/fgi/Reflectance_Library/2013SoS/. Ask the authors for the password to access the data.

References

Aoki, T., Aoki, T., Fukabori, M., Hachikubo, A., Tachibana, Y., and Nishio, F.: Effects of snow physical parameters on spectral albedo and bidirectional reflectance of snow, J. Geophys. Res., 105, 10219–10236, 2000.

Bisiaux, M. M., Edwards, R., McConnell, J. R., Albert, M. R., Anschütz, H., Neumann, T. A., Isaksson, E., and Penner, J. E.: Variability of black carbon deposition to the East Antarctic Plateau, 1800–2000 AD, Atmos. Chem. Phys., 12, 3799–3808, doi:10.5194/acp-12-3799-2012, 2012.

Bond, T. C., Doherty, S. J., Fahey, D. W., Forster, P. M., Berntsen, T., DeAngelo, B. J., Flanner, M. G., Ghan, S., Kärcher, B., Koch, D., Kinne, S., Kondo, Y., Quinn, P. K., Sarofim, M. F., Schultz, M. G., Schulz, M., Venkataraman, C., Zhang, H., Zhang, S., Bellouin, N., Guttikunda, S. K., Hopke, P. K., Jacobson, M. Z., Kaiser, J. W., Klimont, Z., Lohmann, U., Schwarz, J. P., Shindell, D., Storelvmo, T., Warren, S. G., and Zender, C. S.: Bounding the role of black carbon in the climate system: a scientific assessment., J. Geophys. Res.-Atmos., 188, 5380–5552, doi:10.1002/jgrd.50171, 2013.

Bourgeois, C. S., Calanca, P., and Ohmura, A.: A field study of the hemispherical directional reflectance factor and spectral albedo of dry snow, J. Geophys. Res., 111, D20108, doi:10.1029/2006JD007296, 2006.

Brandt, R. E., Warren, S. G., and Clarke, A. D.: A controlled snowmaking experiment testing the relation between black carbon content and reduction of snow albedo, J. Geophys. Res.-Atmos., 116, D08109, doi:10.1029/2010JD015330, 2011.

Clarke, A. D. and Noone, K. J.: Soot in the Arctic snowpack: a cause for perturbations in radiative transfer, Atmos. Environ., 19, 2045–2053, 1985.

Conway, H., Gades, A., and Raymond, C.: Albedo of dirty snow during conditions of melt, Water Resour. Res., 32, 1713–1718, 1996.

Dagsson-Waldhauserova, P., Arnalds, O., Olafsson, H., Hladil, J., Skala, R., Navratil, T., Chadimova, L., and Meinander, O.: Snow-dust storm: unique case study from Iceland, 6–7 March 2013, Aeol. Res., 16, 69–74, doi:10.1016/j.aeolia.2014.11.001, 2015.

Doherty, S. J., Warren, S. G., Grenfell, T. C., Clarke, A. D., and Brandt, R. E.: Light-absorbing impurities in Arctic snow, Atmos. Chem. Phys., 10, 11647–11680, doi:10.5194/acp-10-11647-2010, 2010.

Dumont, M., Brun, E., Picard, G., Michou, M., Libois, Q., Petit, J.-R., Geyer, M., Morin, S., and Josse, B.: Contribution of light-absorbing impurities in snow to Greenland's darkening since 2009, Nat. Geosci., 7, 509–512, doi:10.1038/ngeo2180, 2014.

Fierz, C., Armstrong, R., Durand, Y., Etchevers, P., Greene, E., McClung, D., Nishimura, K., Satyawali, P., and Sokratov, S.: The International Classification for Seasonal Snow on the Ground, no. 83 in IHP-VII Technical Documents in Hydrology, IACS Contribution No. 1, UNESCO-IHP, Paris, 2009.

Flanner, M. G., Zender, C. S., Randerson, J. T., and Rasch, P. J.: Present-day climate forcing and response from black carbon in snow, J. Geophys. Res. Atm., 112, doi:10.1029/2006JD008003, 2007.

Forsström, S., Ström, J., Pedersen, C. A., Isaksson, E., and Gerland, S.: Elemental carbon distribution in Svalbard snow, J. Geophys. Res., 114, D19112, doi:10.1029/2008JD011480, 2009.

Hadley, O. L. and Kirchstetter, T. W.: Black-carbon reduction of snow albedo, Nature Climate Change, 2, 437–440, doi:10.1038/NCLIMATE1433, 2012.

Hakala, T., Suomalainen, J., and Peltoniemi, J. I.: Acquisition of bidirectional reflectance factor dataset using a micro unmanned aerial vehicle and a consumer camera, Remote Sensing, 3, 819–832, doi:10.3390/rs2030819, 2010.

Hakala, T., Riihelä, A., Lahtinen, P., and Peltoniemi, J. I.: Hemispherical-directional reflectance measurements

350   of snow on the Greenland ice sheet during the radiation, snow characteristics and albedo at Summit (RAS-CALS) campaign, J. Quant. Spectrosc. Ra., 146, 376–390, 2014.

Hapke, B.: Theory of Reflectance and Emittance Spectroscopy, Cambridge University Press, Cambridge, 1993.

Kaasalainen, S., Kaasalainen, M., Mielonen, T., Suomalainen, J., Peltoniemi, J., and Näränen, J.: Optical properties of snow in hotspot region, J. Glaciol., 574–584, 2006.

355   Kaspari, S. D., Schwikowski, M., Gysel, M., Flanner, M. G., Kang, S., Hou, S., and Mayewski, P. A.: Recent increase in black carbon concentrations from a Mt. Everest ice core spanning 1860–2000 AD, J. Geophys. Res., 38, L04703, doi:10.1029/2010GL046096, 2011.

Kokhanovsky, A.: Spectral reflectance of solar light from dirty snow: a simple theoretical model and its validation, The Cryosphere, 7, 1325–1331, doi:10.5194/tc-7-1325-2013, 2013.

360   Lyapustin, A., C. K. Gatebe, R. Kahn, R. Brandt, J. Redemann, P. Russell, M. D. King, C. A. Pedersen, S. Gerland, R. Poudyal, A. Marshak, Y. Wang, C. Schaaf, D. Hall, and A. Kokhanovsky: Analysis of Snow Bidirectional Reflectance from ARCTAS Spring-2008 Campaign. Atmos. Chem. Phys., 10, 4359-4375, 2010.

McConnell, J. R., Edwards, R., Kok, G. L., Flanner, M. G., Zender, C. S., Salzman, E. S., Banta, J. R., Pasteris, D. R., Carter, M. M., and Kahl, J. D. W.: 20th century industrial black carbon emissions altered arctic

365   climate forcing, Science, 317, 1381–1384, 2007.

Meinander, O., Kazadzis, S., Arola, A., Riihelä, A., Räisänen, P., Kivi, R., Kontu, A., Kouznetsov, R., Sofiev, M., Svensson, J., Suokanerva, H., Aaltonen, V., Manninen, T., Roujean, J.-L., and Hautecoeur, O.: Spectral albedo of seasonal snow during intensive melt period at Sodankylä, beyond the Arctic Circle, Atmos. Chem. Phys., 13, 3793–3810, doi:10.5194/acp-13-3793-2013, 2013.

370   Meinander, O., Kontu, A., Virkkula, A., Arola, A., Backman, L., Dagsson-Waldhauserová, P., Järvinen, O., Manninen, T., Svensson, J., de Leeuw, G., and Leppäranta, M.: Brief communication: Light-absorbing impurities can reduce the density of melting snow, The Cryosphere, 8, 991–995, doi:10.5194/tc-8-991-2014, 2014.

Ming, J., Cachier, H., Xiao, C., Qin, D., Kang, S., Hou, S., and Xu, J.: Black carbon record based on a shallow

375   Himalayan ice core and its climatic implications, Atmos. Chem. Phys., 8, 1343–1352, doi:10.5194/acp-8-1343-2008, 2008.

Nicodemus, F. E., Richmond, J. C., Hsia, J. J., Ginsberg, I. W., and Limperis, T.: Geometrical considerations and nomenclature for reflectance, Tech. rep., Institute for Basic Standards, National Bureau of Standards, Washington DC, USA, 1977.

380   Painter, T. H., Dozier, J., Roberts, D. A., Davis, R. E., and Green, R. O.: Retrieval of subpixel snow-covered area and grain size from imaging spectrometer data, Remote Sens. Environ., 85, 64–77, 2003.

Peltoniemi, J., Hakala, T., Suomalainen, J., and Puttonen, E.: Polarised bidirectional reflectance factor measurements from snow, soil and gravel, J. Quant. Spectrosc. Ra., 110, 1940–1953, doi:10.1016/j.jqsrt.2009.04.008, 2009.

Peltoniemi, J., Gritsevich, M., and Puttonen, E.: Reflectance and polarisation characteristics of various vegetation types, in: Light Scattering Reviews, vol. 9, edited by: Kokhanovsky, A., Springer praxis books, Heidelberg, doi:10.1007/978-3-642-37985-7_7, 257–294, 2015.

Peltoniemi, J. I.: Spectropolarised ray-tracing simulations in densely packed particulate medium, J. Quant. Spectrosc. Ra., 108, 180–196, 2007.

Peltoniemi, J. I., Manninen, T., Suomalainen, J., Hakala, T., Puttonen, E., and Riihelä, A.: Land surface albedos computed from BRF measurements with a study of conversion formulae, Remote Sensing, 2, 1918–1940, doi:10.3390/rs2081918, 2010a.

Peltoniemi, J. I., Suomalainen, J., Hakala, T., Puttonen, E., Näränen, J., Kaasalainen, S., Torppa, J., and Hirschmugl, M.: Reflectance of various snow types: measurements, modelling and potential for snow melt monitoring, chap. 9, in: Light Scattering Reviews 5: Single Light Scattering and Radiative Transfer, edited by: Kokhanovsky, A. A., Springer Praxis Books, Heidelberg, doi:10.1007/978-3-642-10336-0, 393–450, 2010b.

Peltoniemi, J. I., Hakala, T., Suomalainen, J., Honkavaara, E., Markelin, L., Gritsevich, M., Eskelinen, J., Jaanson, P., and Ikonen, E.: A detailed study for the provision of measurement uncertainty and traceability for goniospectrometers, J. Quant. Spectrosc. Ra., 146, 376–390, 2014.

Piironen, J., Muinonen, K., Keränen, S., Karttunen, H., and Peltoniemi, J. I.: Backscattering of light from snow: field measurements, in: Observing Land From Space: Science, Customers and Technology, vol. 4 of Advances in Global Change Research, edited by: Verstraete, M. M., Menenti, M., and Peltoniemi, J. I., 219-228, Kluwer, Dordrecht, the Netherlands, 2000.

Räisänen, P., Kokhanovsky, A., Guyot, G., Jourdan, O., and Nousiainen, T.: Parameterization of single-scattering properties of snow, The Cryosphere Discuss., 9, 873–926, doi:10.5194/tcd-9-873-2015, 2015.

Sasse, C. and Peltoniemi, J. I.: Angular scattering measurements and calculations of rough spherically shaped carbon particles, in: Opt. Sci., and Sci. Instr., SPIE, doi:10.1117/12.218329, 1995.

Suomalainen, J., Hakala, T., Peltoniemi, J., and Puttonen, E.: Polarised multiangular reflectance measurements using Finnish Geodetic Institute Field Goniospectrometer, Sensors, 9, 3891–3907, doi:10.3390/s90503891, 2009.

Svensson, J., Ström, J., Hansson, M., and Lihavainen, H.: Observed metre scale horizontal variability of elemental carbon in surface snow, Environ. Res. Lett., 8, doi:10.1088/1748-9326/8/3/034012, 034012, 2013.

Svensson, J., Virkkula, A., Meinander, O., Kivekäs, N., Hannula, H.-R., Järvinen, O., Peltoniemi, J. I., Gritsevich, M., Heikkilä, A., Kontu, A., Hyvärinen, A.-P., Neitola, K., Brus, D., Dagsson-Waldhauserova, P., Anttila, K., Hakala, T., Kaartinen, H., Vehkamäki, M., de Leeuw, G., and Lihavainen, H.: Soot on snow experiments: light-absorbing impurities effect on the natural snowpack, The Cryosphere Discuss., 9, 1227–1267, doi:10.5194/tcd-9-1227-2015, 2015.

Tanikawa, T., Aoki, T., Hori, M., Hachikubo, A., and Aniya, M.: Snow bidirectional reflectance model using non-spherical snow particles and its validation with field measurements, EARSeL eProceedings, 5, 137–145, 2006.

Tanikawa, T., Hori, M., Aoki, T., Hachikubo, A., Kuchiki, K., Niwano, M., Matoba, S., Yamaguchi, S., and Stamnes, K.: In situ measurements of polarization properties of snow surface under the Brewster

13

Table 1. List of the samples measured using FIGIFIGO during the SoS campaign at the Sodankylä airport. Numbers in parenthesis are from unstable data, double parenthesis denoting very unstable data, due to increasing cloudiness. ID means the name by which the measurement is found in the data base, SZA the solar zenith angle, and PAR alb. the albedo integrated over the photosynthetically active range.

Start time	sample	SZA	ID	albedo	PAR alb
3 Apr 2013 11:33	clean soft snow	63	1	0.80	0.96
3 Apr 2013 12:25	snow + volcanic sand, 8 g	62	56	0.78	0.93
3 Apr 2013 13:23	snow + volcanic sand, 8 g	62	2	(0.72)	(0.86)
3 Apr 2013 14:42	snow clean	64	3	0.74	0.87
4 Apr 2013 9:56	snow + soot, 1 kg/+ new snow < 1 mm	68	5	0.68	0.83
4 Apr 2013 10:31	snow + soot, 1 kg/+ new snow < 1 mm	66 p	5 P	((0.74))	((0.94))
4 Apr 2013 11:18	snow + soot, 1 kg/+ new snow < 1 mm	62 p	55	0.65	0.80
4 Apr 2013 12:39	snow + soot, 1 kg/+ new snow < 1 mm	63 p	6	0.65	0.84
4 Apr 2013 13:31	clean snow	62	7	0.76	0.94
4 Apr 2013 15:05	snow + silt, 10 g	65	8	0.70	0.83
4 Apr 2013 16:39	snow + silt, 20 g	72	9	0.46	0.51
5 Apr 2013 11:16	snow + silt, 20 g	61	10	0.41	0.51
5 Apr 2013 14:16	snow + silt, 40 g	62	11	(0.17)	(0.20)
5 Apr 2013 15:08	clean snow	66	12	(0.78)	(0.96)
5 Apr 2013 16:55	snow + silt, 40 g	74	13	((0.22))	((0.23))

geometry in Hokkaido, Japan, and northwest Greenland ice sheet, J. Geophys. Res., 119, 13946–13964, doi:10.1002/2014JD022325, 2014.

Warren, S.: Can black carbon in snow be detected by remote sensing?, J. Geophys. Res.-Atmos., 118, 779–786, 2013.

Warren, S. and Wiscombe, W.: A model for spectral albedo of snow II: Snow containing atmospheric aerosols, J. Atmos. Sci., 37, 2734–2747, 1980.

Wiscombe, W. and Warren, S.: A model for spectral albedo of snow I: Pure snow, J. Atmos. Sci., 37, 2712–2733, 1980.

Xu, B., Cao, J., Hansen, J., Yao, T., Joswiak, D., Wang, N., Wu, G., Wang, M., Zhao, H., Yang, W., Liu, X., and He, J.: Black soot and the survival of Tibetan glaciers, P. Natl. Acad. Sci. USA, 106, 22114–22118, 2009.

Table 2. The snow structure profile, 3 April 2013 11:20. Snow depth from the snow pack surface [cm], snow grain shape, hand hardness index, and snow wetness index defined according to Fierz et al. (2009). Minimum, maximum, and average snow grain size ([mm], longest axis, 0.25 mm resolution) as visually approximated from macro-photographs.

Depth [cm]	crystal shape	hardness	wetness	min size [mm]	max size	average size
3	Ppir	1	2	0.0	1.0	0.3
16	RGxf	1	1	0.5	1.5	0.8
20	RGxf	1	1	0.3	1.8	1.0
31	Fcso	1	1	0.5	2.5	1.0
39	FCso	2	1	0.5	2.3	1.3
52	DHcp + DHch	1	1	0.5	4.0	1.5
66	DHcp	4	1	0.0	4.3	2.3

Table 3. The snow density profile, measured at the Sodankylä airport near FIGIFIGO spot on 3 April 2013 15:00.

Depth [cm]	density [$\mathrm{g\,cm^{-3}}$]
0–5	0.244
5–10	0.272
10–15	0.256
15–20	0.248
20–25	0.256
25–30	0.300
30–35	0.300
45–40	0.244
40–45	0.292
45–50	0.324
50–55	0.232

Table 4. Snow depth profile measured from a snow pit 5 April 2013.

Depth [cm]	crystal shape	
surface	PPir	small crystalline, not dendr. edgy, smaller than 3 Apr
1.5	RGxf	more icy, more granular
4	FCsf	even more icy, grains larger
12.5	FCsf	similar
15	FCco	ice lens below harder
19	MFcf	rough icy grains
29	FCso	larger icy grains
32	FCso	below harder
42	FCso+DHcp	larger icy grains
47	DHcp+DHch	larger faceted icy grains
59	DHcp+DHch	larger icy grains, planar
64	DHcp+DHch	icy deep choar

Table 5. The snow density profile, measured at the airport near the FIGIFIGO spot on 5 April 2013.

Depth [cm]	density [$\mathrm{g\,cm^{-3}}$]	comment
0–5	0.29	icy
5–10	0.36	harder
10–15	0.28	
15–20	0.24	
20–25	0.24	
25–30	0.30	
30–35	0.30	
35–40	0.25	
40–45	0.28	
45–50	0.28	
50–55	0.25	
55–60	0.24	
59–64	0.22	
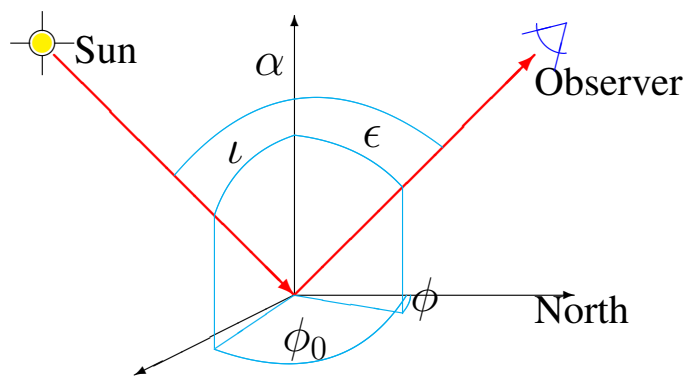
Figure 1. Definition of the angles used in surface reflectance work: ϵ and ι are the zenith angles of the emergent (Observer) and incident (solar) radiation respectively (shorthand $\mu = \cos\epsilon$ and $\mu_0 = \cos\iota$ are also used). ϕ and ϕ_0 are the corresponding azimuth angles. The phase angle α is the angle between the observer and the Sun. The principal plane is fixed by the solar direction and the surface normal, while the cross plane is a vertical plane perpendicular to the principal plane.

Figure 2. FIGIFIGO at the SoS test site at the Sodankylä airport. A clean snow sample has been measured, and the last reference measurement with the white Spectralon panel is being taken. Deep and soft snow complicated the usability of FIGIFIGO. While the movements in the snow left significant traces, the target area under the instrument footprint was carefully kept untouched during the measurement.

Figure 3. Photographs of the samples. Left an overview, right some details. From the top, clean snow 4 April 2013, snow deposited with volcanic ash 3 April 2013, snow deopsited with chimney soot 4 April 2013, and on the bottom snow deposited with glaciogenic silt 4 April 2013.

Figure 4. More snow profiles taken on the 3 April of unprocessed snow near the FIGIFIGO spot. Because of near zero temperature, the snow crystals melt fast on the black plate, and the smallest details and grains have already disappeared.

Figure 5. More snow profiles taken on the 4 April of unprocessed snow near the FIGIFIGO spot, plus one profile from the sample sooted on the 3 April, and measured on the 4 April.
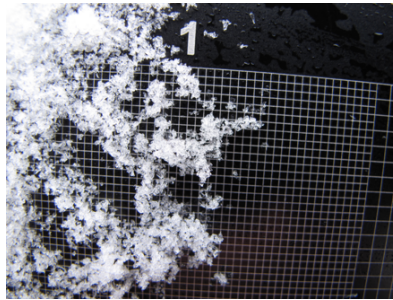
Figure 6. More snow profiles taken on the 5 April of unprocessed snow near the FIGIFIGO spot.
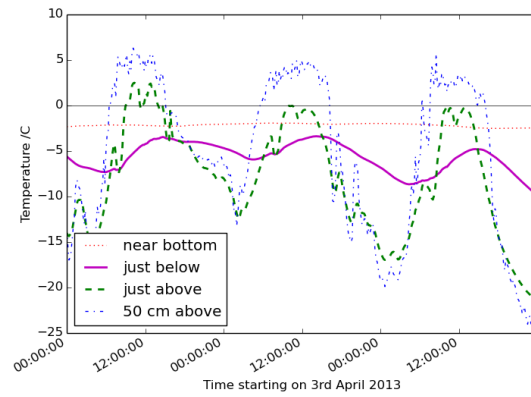
Figure 7. The snow and air temperatures measured by an FMI weather station at a swamp near Tähtelä, Sodankylä, few kilometers from the airport. The bottom value is measured at the interface between snow and ground, "just below" is 1–9cm below the snow surface, and "just above" 9–1cm above.
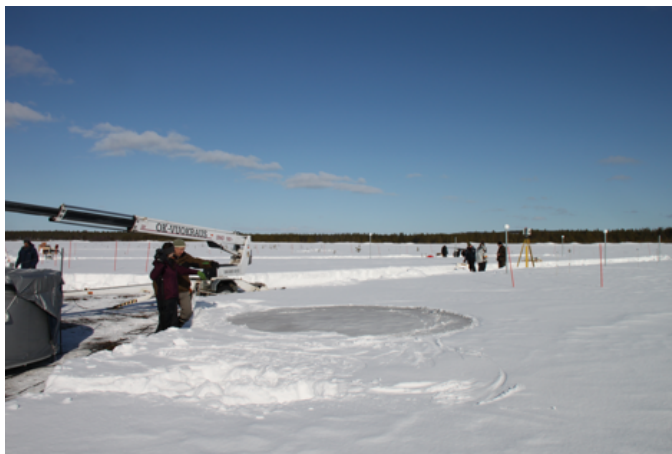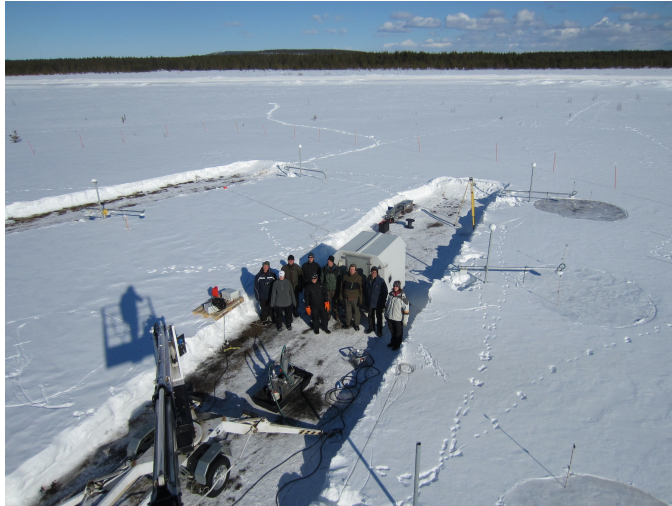
Figure 8. The SoS experiment system in Sodankylä airport. Top photo by Rae Ellen Bichell.
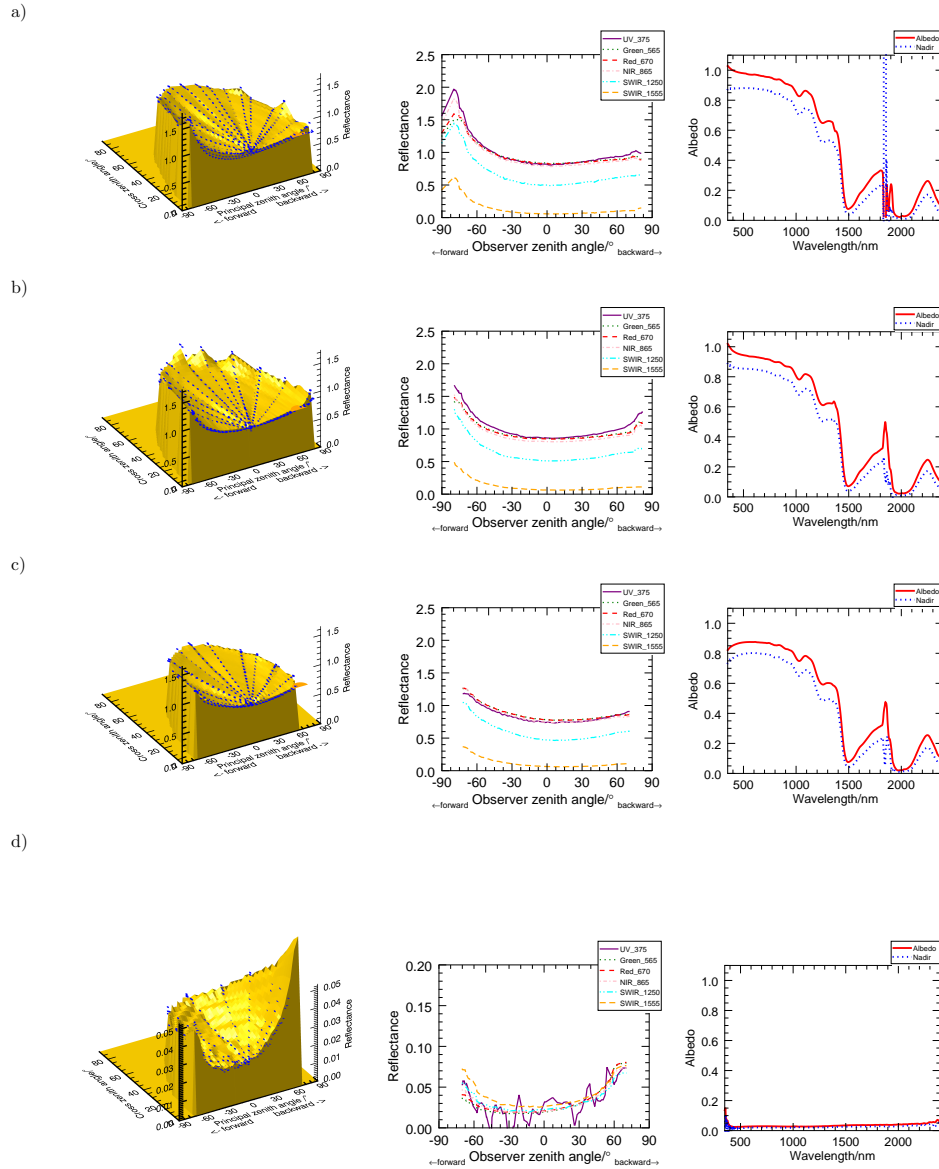
Figure 9. Left: BRF as a function of the observation direction integrated over the spectral range. Middle: The bidirectional reflectance factor (BRF) in the principal plane, at six wavelengths. Right: spectral albedo and BRF at nadir. **(a)** Natural snow 3 April 2013 11:33, SZA $63°$, **(b)** snow covered with volcanic sand, $8\,\mathrm{g}/0.5\,\mathrm{m}^2$, 3 April 2013, 12:25, $62°$, **(c)** snow covered with volcanic sand, $8\,\mathrm{g}/0.5\,\mathrm{m}^2$, 3 April 2013 13:23, $62°$, **(d)** pure volcanic sand measured in laboratory.
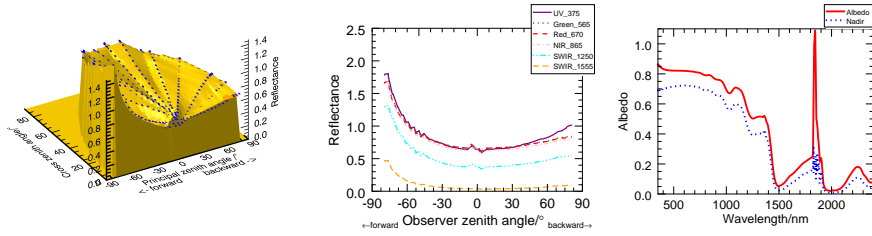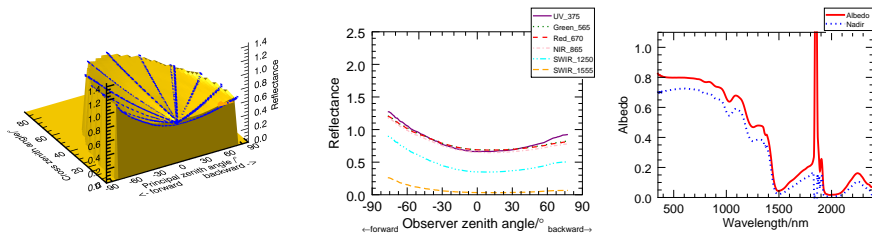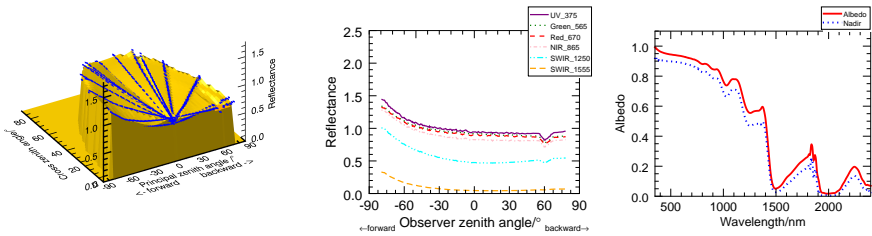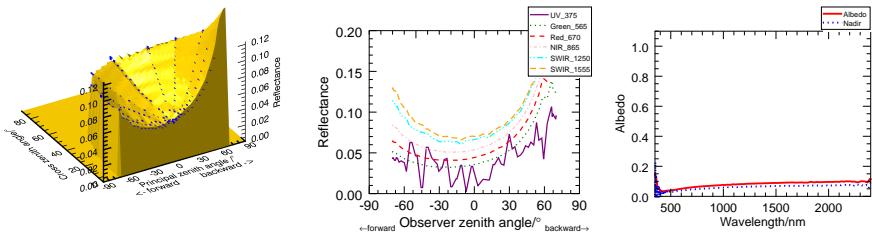
Figure 10. As in Fig. 9. Sooted snow on the 4 April 2013. **(a)** started at 9:56 with 68° SZA; **(b)** 10:31, 62°, **(c)** 11:18, 63°, **(d)** natural snow sample at 13:31, 62°.
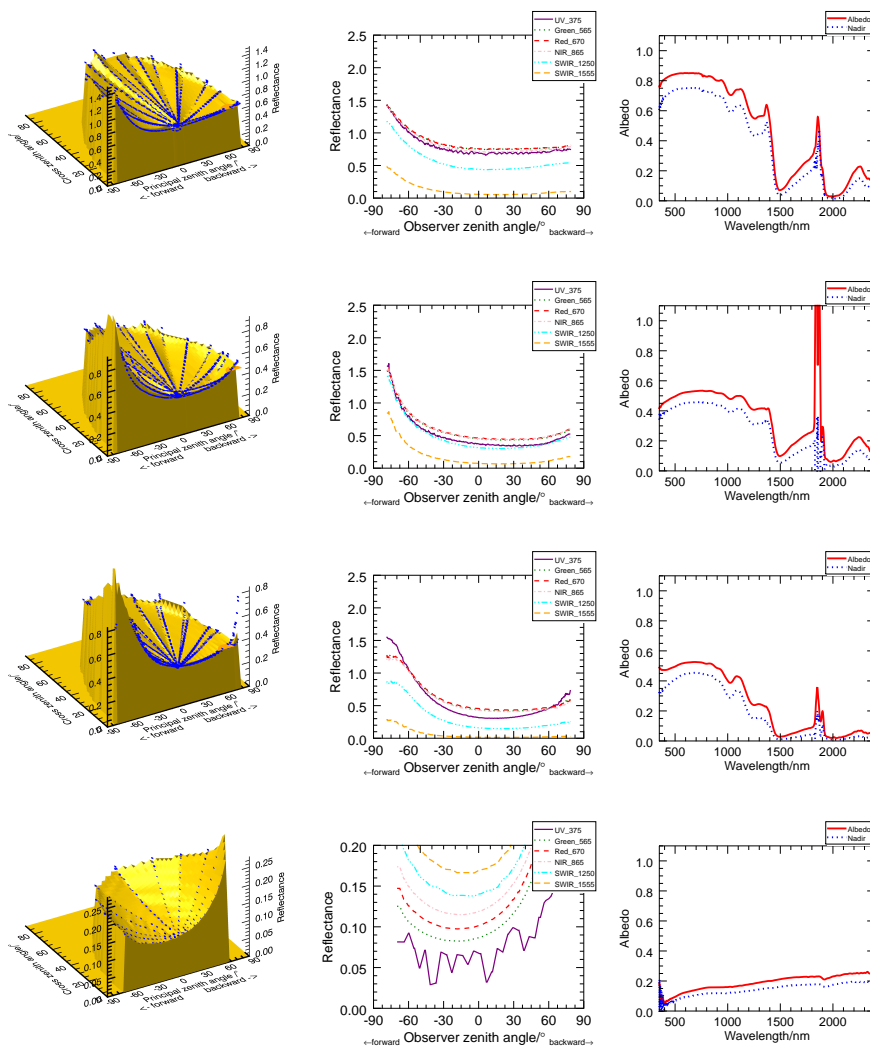
26

Figure 11. As in Fig. 9. **(a)** 10 g of silt /0.5 m^2 on top of snow, on the 4 April 2013 at 15:05, 65°, **(b)** 10 g of silt/0.5 m^2, on the 4 April 2013 at 16:29, 72°, note large SZA, **(c)** same sample on the 5 April 2013 at 11:16, 61°, most difference to b due to different SZA, **(d)** pure silt measured in laboratory, 65°.
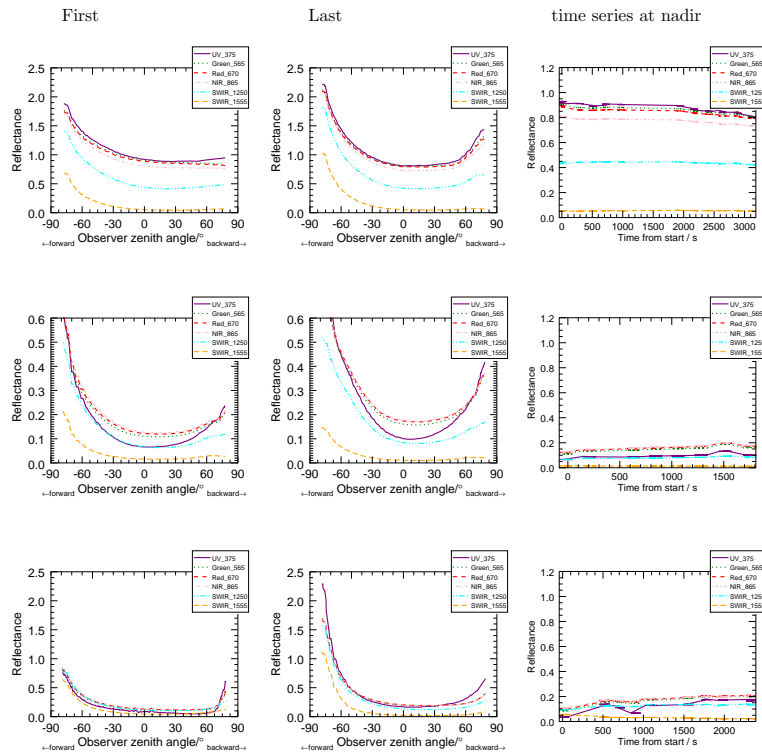
Figure 12. How the reflectance changes during the measurements. Left plot, the reflectance in the principal plane measured in the beginning of a sequence, and in the middle the same measured at the end of the sequence. On the right is the reflectance in nadir taken at different time steps. The top is untouched snow, the middle is snow with fine silt $40\,\mathrm{g}/0.5\,\mathrm{m}^2$, taken at $62°$, and the bottom taken at $74°$. Untouched snow darkens a little bit at nadir and brightens at large zenith angles, while contaminated snow brightens clearly in all directions, especially at large zenith angles.